Hindcasting to measure ice sheet model sensitivity to initial states: Supplement

A. Aschwanden, G. Aðalgeirsdóttir, C. Khroulev

1 Climate Forcing

The hydrostatic atmospheric regional climate model HIRHAM5 (Christensen et al., 2006) provides monthly mean climatic mass balance and 2-m air temperature. HIRHAM is based on HIRLAM7 dynamics (Eerola, 2006) and ECHAM5 physics (Roeckner et al., 2003). HIRHAM5 is forced at the lateral boundaries using the European Centre for Medium-Range Weather Forecasts ERA-Interim reanalysis product (Dee et al., 2011) for the period 1989–2011. The regional climate model dynamically downscales the temperature and precipitation fields and computes the climatic mass balance at a resolution of 0.05° (∼5.55 km) with 31 vertical levels and a time-step of 120 s in the dynamical scheme. HIRHAM5 has been validated both with ice core data and automatic weather station data and is shown to perform well over Greenland (Dethloff et al., 2002; Kiilsholm et al., 2004; Lucas-Picher et al., 2012; Rae et al., 2012). At present, formal error estimates are not available due to the lack of sufficient observations.

2 Ice Sheet Model

Simulations are performed with the open-source Parallel Ice Sheet Model (PISM, www.pism-docs.org)[1], which is thermomechanically-coupled, polythermal, and includes a hybrid stress balance model (Bueler and Brown, 2009; Aschwanden et al., 2012). PISM has been used in a number of studies of the ice sheets on Greenland and Antarctica (e.g., Martin et al., 2011; Solgaard et al., 2011; Solgaard and Langen, 2012; Golledge et al., 2012).

At the ocean boundary, ice is calved-off at the initial calving position, which is held fixed throughout the simulations. Basal topography and ice thickness are from Griggs et al. (2012). At the basal boundary, geothermal flux varies in space (Shapiro and Ritzwoller, 2004), and a nearly-plastic power law (Schoof and Hindmarsh, 2010) relates bed-parallel shear stress, $\boldsymbol{\tau}_b$, and the sliding velocity, $\mathbf{u}_b$:

$$\boldsymbol{\tau}_b = -\tau_c \frac{\mathbf{u}_b}{|\mathbf{u}_b|^{(1-q)} u_0^q}, \tag{2.1}$$

where τ_c is the yield stress, q is the pseudo-plasticity exponent, and $u_0 = 100\,\mathrm{m\,a^{-1}}$ is a threshold speed. The basal material (till) is partially water saturated. Saturation, yield stress and modeled liquid water pressure within the till are related by the pore water pressure, p_w, given as a fraction of the overburden pressure:

$$p_w = \alpha\, w \rho g H \qquad \text{in} \qquad \tau_c = (\tan\phi)(\rho g H - p_w). \tag{2.2}$$

Here, H is the ice thickness, $\rho g H$ is the overburden pressure, and ϕ is the till friction angle. The relative amount of stored water in the till, w, comes from time-integrating the basal melt rate. Excess water drains when the thickness of stored water reaches 2 m. The coefficient α is the allowed pore water pressure fraction. The yield stress τ_c is also a function of the till friction angle ϕ, prescribed as a continuous function of the bed elevation, with $\phi = 5^\circ$ for bed elevations lower than 300 m below sea level, $\phi = 20^\circ$ for bed locations higher than 700 m above sea level, and changing linearly in between.

The enhancement factor, E, is a simple tuning parameter for ice dynamics. This factor is commonly used in ice sheet models to change the ice flow properties to account for the effect of the anisotropic nature of ice as well as impurities. The enhancement factor appears in the definition of the effective viscosity of glacier ice, η,

$$2\eta = (E\,A)^{-1} \left(\tau_{\mathrm{e}}^2 + \epsilon^2\right)^{\frac{1-n}{2n}}, \tag{2.3}$$

where τ_{e} is the effective stress, A is the rate factor (softness), and $n = 3$ is the exponent of the power law. The small constant ϵ (units of stress) regularizes the flow law at low effective stress, avoiding the problem of infinite viscosity at zero deviatoric stress.

[1] All simulations used development revision `c52bdfd`

The three tuning parameters that are used to obtain a close fit to the observed surface speed are the enhancement factor E, the pseudo-plasticity exponent q, and the allowed pore water pressure fraction α. We use $(E, q, \alpha) = (3, 0.25, 0.95)$.

The three initialization procedures start from the same model state, obtained by running the model at a 20 km horizontal grid resolution with constant surface forcing for 50 ka while keeping the geometry fixed.

Horizontal and vertical model resolutions are 2 km and 10 m, respectively. The computational domain extends horizontally over 1500 km $\times$ 2800 km, and vertically over 4000 m and 2000 m in the ice and in the bedrock, respectively. For computational efficiency grid refinements are made during the initialization procedure. The runs are started on a 20 km grid, then refined from 20 km to 10 km at at -7'000 a, to 5 km at -2'000 a, to 2.5 km at -850 a, and finally to 2 km at -350 a. However, all the runs continue on their respective resolutions such that all initializations are available on all the listed grid resolutions. The run lengths are sufficiently long to remove unphysical transient noise resulting from the grid-refinement. Basal topography is remapped onto the respective grids using a first-order conservative algorithm. The correlation coefficient is consistent for all grid resolutions (Table 4.3). PISM uses an adaptive time-stepping scheme, and typical time-steps are about 2 days for a horizontal grid resolution of 2 km.

3 Flux-correction

The flux-correction method explained below is applied during the last 2,000 years of the flux-corrected paleo-climate initialization.

To obtain an ice sheet geometry in closer agreement with measurements we modify the climatic mass balance M. Let H_{tar} be this target ice thickness, and let H be the current model thickness. Recall that the mass continuity equation is

$$\frac{\partial H}{\partial t} = M - S - \nabla \cdot \mathbf{q}, \tag{3.1}$$

where M and S are the surface and basal mass balance, respectively, and $\nabla \cdot \mathbf{q}$ is the flux divergence. Replacing M with the modified surface mass balance yields the modified continuity equation

$$\frac{\partial H}{\partial t} = \tilde{M} - S - \nabla \cdot \mathbf{q}, \tag{3.2}$$

with

$$\tilde{M} = M + \Delta M = M + \beta \left(H_{\text{tar}} - H \right), \tag{3.3}$$

where $\beta > 0$ is set to $0.05\,\text{a}^{-1}$. To reduce the shock arising from a switch in climate at the transition between initialization and hindcast, we apply the climate forcing during the hindcast as anomalies. Let χ and χ_{init} be the climate of the hindcast and the average of the last 10 years of the initialization, respectively. Then, the hindcast climate for the simulation based on "flux-corrected" initial state $\tilde{\chi}$ is

$$\tilde{\chi} = \chi_{\text{init}} + \left(\chi - \chi_0 \right), \tag{3.4}$$

where χ_0 is the climate at the beginning of the hindcast (1 Jan 1989). Figure 3.1 shows the climatic mass balance of the last 10 years of the initialization for all three initialization methods. Largest differences occur in coastal areas and on small glaciers and ice caps.

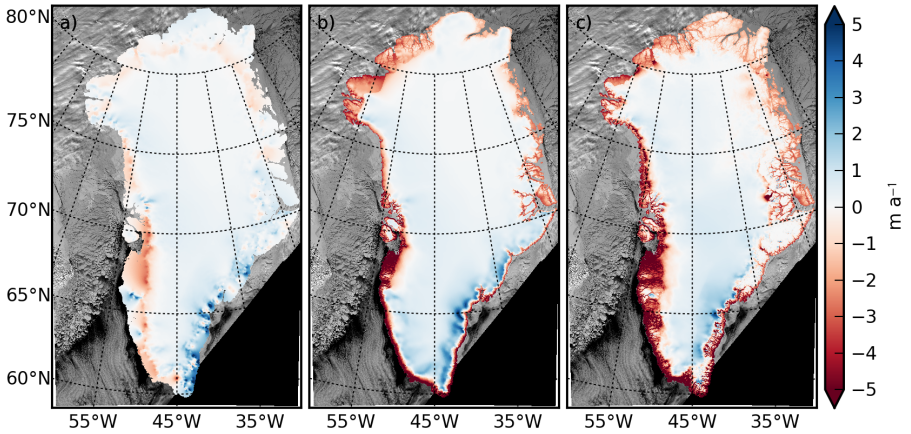

Figure 3.1: Mean climatic mass balance of the last 10 years of the initialization. **(a)** "constant-climate". **(b)**. "paleo-climate". **(c)** "flux-corrected".

4 Supplementary Figures and Tables

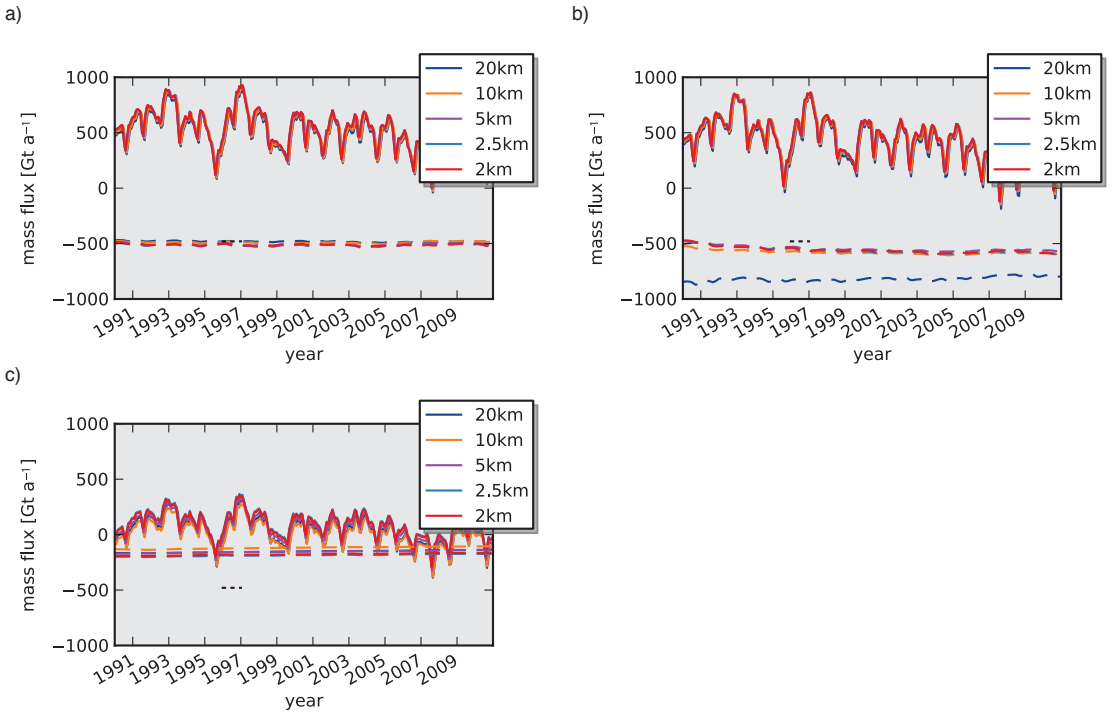

Figure 4.1: Simulated mass fluxes as a function of grid resolution from 1990 to 2008. a) constant-climate hindcast. b) paleo-climate hindcast. c) flux-corrected hindcast. Climatic mass balance (solid line) and ice discharge (dashed line). For comparison the ice discharge estimate for 1996 (van den Broeke et al., 2009) is shown (black dotted line). Time-series are smoothed with a 13-month running-average filter.

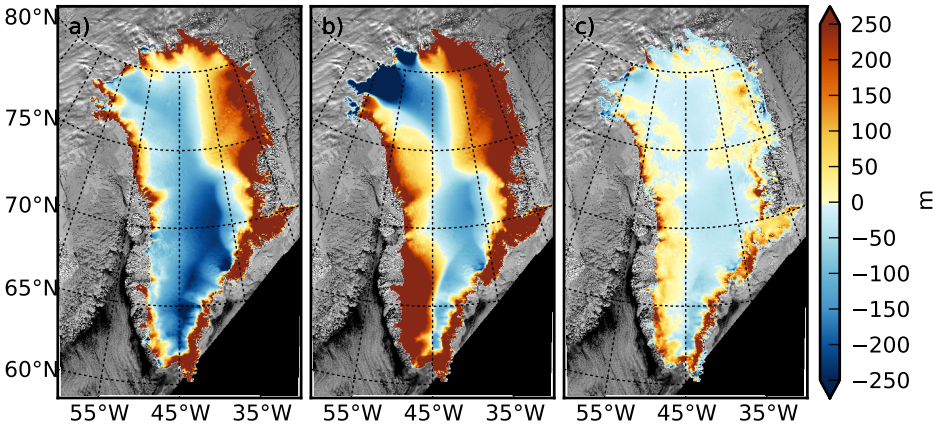

Figure 4.2: Absolute difference in ice thickness (model-observation). a) constant-climate initialization. b) paleo-climate initialization. c) flux-corrected paleo-climate initialization; ice thickness was used in the initialization, hence only shown for comparison. Blue and red colors indicate the model under- and over-estimates ice thickness, respectively.

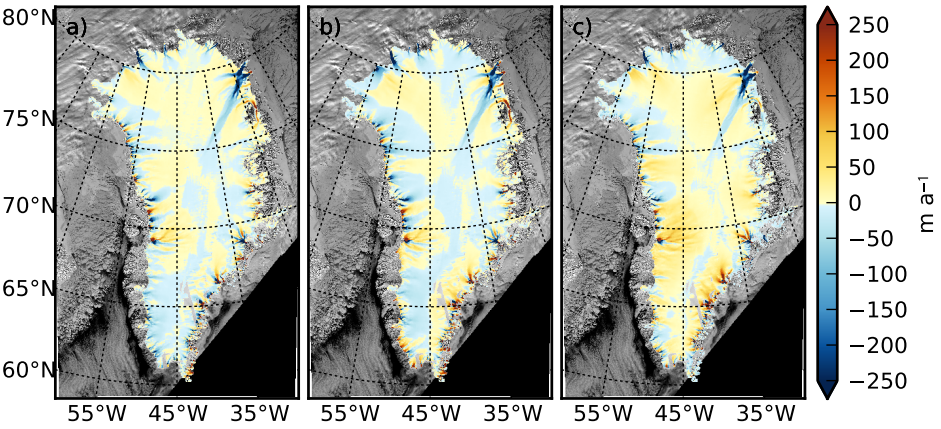

Figure 4.3: Absolute difference in surface speeds (model-observation). a, constant-climate initialization. b, paleo-climate initialization. c, flux-corrected paleo-climate initialization. Blue and red colors indicate the model under- and over-estimates surface speed, respectively.

Table 4.1: Root mean square error (RMSE, units $\mathrm{m\,a^{-1}}$) of simulated surface speeds of the inital state (1989) and at the end of the hindcast (2011) compared to observed surface speeds of 2006–2009, 2006, and 2008.

simulation	observation	"constant-climate"	"paleo-climate"	"flux-corrected"
1989	2006–2009	43	46	45
1989	2006	45	48	47
1989	2008	45	47	47
2011	2006–2009	43	45	46
2011	2006	45	47	48
2011	2008	45	48	46

Table 4.2: Mass loss trend b as a function of horizontal grid resolution g. Mean $\bar{b}$ and standard deviation b_σ of the mass loss rates are also listed.

g [km]	b [$\mathrm{Gt\,a^{-1}}$]		
	"constant-climate"	"paleo-climate"	"flux-corrected"
20	-143	-557	-234
10	-128	-323	-214
5	-136	-288	-205
2.5	-137	-303	-199
2	-139	-299	-198
$\bar{b}$	-140	-361	-210
b_σ	5	102	14

Table 4.3: Correlation coefficient, r, of the correlation between simulated and observed mass loss time series as a function of horizontal grid resolution, g.

g [km]	r [-]		
	"constant-climate"	"paleo-climate"	"flux-corrected"
20	0.910	0.984	0.882
10	0.883	0.977	0.882
5	0.918	0.984	0.988
2.5	0.920	0.986	0.989
2	0.919	0.986	0.988

Bibliography

Aschwanden, A., Bueler, E., Khroulev, C., and Blatter, H.: An enthalpy formulation for glaciers and ice sheets, J. Glaciol., 58, 441–457, doi:10.3189/2012JoG11J088, 2012.

Bueler, E. and Brown, J.: The shallow shelf approximation as a "sliding law" in a thermomechanically coupled ice sheet model, J. Geophys. Res., 114, 1–21, doi:10.1029/2008JF001179, 2009.

Christensen, O. B., Drews, M., Dethloff, K., Ketelsen, K., Hebestadt, I., and Rinke, A.: The HIRHAM Regional Climate Model. Version 5. Tech. Report 06-17, Tech. rep., DMI, Copenhagen, 2006.

Dee, D. P., Uppala, S. M., Simmons, A. J., Berrisford, P., Poli, P., Kobayashi, S., Andrae, U., Balmaseda, M. A., Balsamo, G., Bauer, P., Bechtold, P., Beljaars, A. C. M., van de Berg, L., Bidlot, J., Bormann, N., Delsol, C., Dragani, R., Fuentes, M., Geer, A. J., Haimberger, L., Healy, S. B., Hersbach, H., Hólm, E. V., Isaksen, L., Kållberg, P., Köhler, M., Matricardi, M., McNally, A. P., Monge-Sanz, B. M., Morcrette, J.-J., Park, B.-K., Peubey, C., de Rosnay, P., Tavolato, C., Thépaut, J.-N., and Vitart, F.: The ERA-Interim reanalysis: configuration and performance of the data assimilation system, Q. J. Roy. Meteor. Soc., 137, 553–597, doi:10.1002/qj.828, 2011.

Dethloff, K., Schwager, M., Christensen, J. H., Kiilsholm, S., Rinke, A., Dorn, W., Jung-Rothenhäusler, F., Fischer, H., Kipfstuhl, S., and Miller, H.: Recent Greenland accumulation estimated from Regional Climate model simulations and ice core analysis, J. Climate, 15, 2821–2832, 2002.

Eerola, K.: About the performance of the Hirlam version 7.0. Tech. Rep. 51, Article 14, Tech. Rep. 51, DMI, Copenhagen, 2006.

Golledge, N. R., Fogwill, C. J., Mackintosh, A. N., and Buckley, K. M.: Dynamics of the last glacial maximum Antarctic ice-sheet and its response to ocean forcing, P. Natl. Acad. Sci. USA, pp. 1–5, doi:10.1073/pnas.1205385109, 2012.

Griggs, J. A., Bamber, J. L., , Hurkmans, R. T. W. L., Dowdesewell, J. A., Gogineni, S. P., Howat, I., Mouginot, J., Paden, J., Palmer, S., Rignot, E., and Steinhage, D.: A new bed elevation dataset for Greenland, The Cryosphere Discussions, 6, 4829–4860, doi:10.5194/tcd-6-4829-2012, URL `http://www.the-cryosphere-discuss.net/6/4829/2012/`, 2012.

Kiilsholm, S., Christensen, J. H., Dethloff, K., and Rinke, A.: Net accumulation of the Greenland ice sheet: High resolution modeling of climate changes, Geophys. Res. Lett., 30, doi:10.1029/2002GL015742, 2004.

Lucas-Picher, P., Wulff-Nielsen, M., Christensen, J. H., Aðalgeirsdóttir, G., Mottram, R., and Simonsen, S. B.: Very high resolution regional climate model simulations over Greenland: Identifying added value, J. Geophys. Res., 117, doi: 10.1029/2011JD016267, 2012.

Martin, M. A., Winkelmann, R., Haseloff, M., Albrecht, T., Bueler, E., Khroulev, C., and Levermann, A.: The Potsdam Parallel Ice Sheet Model (PISM-PIK) Part 2: Dynamic equilibrium simulation of the Antarctic ice sheet, The Cryosphere, 5, 727–740, doi:10.5194/tc-5-727-2011, 2011.

Rae, J. G. L., Aðalgeirsdóttir, G., Edwards, T. L., Fettweis, X., Gregory, J. M., Hewitt, H. T., Lowe, J. a., Lucas-Picher, b., Mottram, R. H., Payne, a. J., Ridley, J. K., Shannon, S. R., van de Berg, W. J., van de Wal, R. S. W., and van den Broeke, M. R.: Greenland ice sheet surface mass balance: evaluating simulations and making projections with regional climate models, The Cryosphere, 6, 1275–1294, doi:10.5194/tc-6-1275-2012, URL http://www.the-cryosphere.net/6/1275/2012/, 2012.

Roeckner, E., Bäuml, G., Bonaventura, L., Brokopf, R., Esch, M., Giorgetta, M., Hagemann, S., Kirchner, I., Kornblueh, L., Manzini, E., Rhodin, A., Schlese, U., Schulzweida, U., and Tompkins, A.: The atmospheric general circulation model ECHAM5. Part I: model description, Tech Rep. 349, Tech. Rep. 349, Max-Planck Institute for Meteorology, Hamburg, 2003.

Schoof, C. and Hindmarsh, R. C. A.: Thin-Film Flows with Wall Slip: An Asymptotic Analysis of Higher Order Glacier Flow Models, Q. J. Mech. Appl. Math., 63, 73–114, doi:10.1093/qjmam/hbp025, 2010.

Shapiro, N. M. and Ritzwoller, M. H.: Inferring surface heat flux distributions guided by a global seismic model: particular application to Antarctica, Earth Planet. Sc. Lett., 223, 213–224, 2004.

Solgaard, A. M. and Langen, P. L.: Multistability of the Greenland Ice Sheet and the effects of an adaptive mass balance formulation, Clim. Dyn., 2012.

Solgaard, A. M., Reeh, N., Japsen, P., and Nielsen, T.: Snapshots of the Greenland ice sheet configuration in the Pliocene to early Pleistocene, J. Glaciol., 57, 871–880, doi:10.3189/002214311798043816, 2011.

van den Broeke, M. R., Bamber, J. L., Ettema, J., Rignot, E., Schrama, E., van de Berg, W. J., van Meijgaard, E., Velicogna, I., and Wouters, B.: Partitioning recent Greenland mass loss, Science, 326, 984–986, doi:10.1126/science.1178176, 2009.